Front. Phys. 10, 107101 (2015)
DOI 10.1007/s11467-015-0496-7

RESEARCH ARTICLE

First-principles investigation of structural, mechanical, electronic, and bonding properties of NaZnSb

Jian-Bing Gu[1,2], Chen-Ju Wang[1,3], Lin Zhang[1,†], Yan Cheng[2], Xiang-Dong Yang[3]

[1] *Laboratory for Shock Wave and Detonation Physics Research, Institute of Fluid Physics, Chinese Academy of Engineering Physics, Mianyang 621999, China*

[2] *College of Physical Science and Technology, Sichuan University, Chengdu 610064, China*

[3] *Institute of Atomic and Molecular Physics, Sichuan University, Chengdu 610065, China*

Corresponding author. E-mail: †zhanglinbox@263.net

Received January 21, 2015; accepted April 12, 2015

The structural, mechanical, electronic, and bonding properties and phase transition of NaZnSb are explored using the generalized gradient approximation based on ab initio plane-wave pseudopotential density functional theory. With the help of the quasi-harmonic Debye model, we probe the Grüneisen parameter, thermal expansivity, heat capacity, Debye temperature, and entropy of NaZnSb in the tetragonal phase. The results indicate that the lattice constants and the bulk modulus and its first pressure derivative agree well with the available theoretical and experimental data. NaZnSb in its ground state structure exhibits a distinct energy gap of about 0.41 eV, which increases with increasing pressure. Our conclusions are consistent with the theoretical predictions obtained by the ABINIT package, but are different from those obtained through the tight-binding linear muffin-tin orbital method. As a result, further experimental and theoretical researches need to be carried out. For the purpose of providing a comparative and complementary study for future research, we first investigate the thermodynamic properties of NaZnSb.

Keywords density functional theory, structural properties, mechanical properties, electronic properties

PACS numbers 71.15.Mb, 71.20.-b, 61.50.Ks, 62.20.-x

1 Introduction

The half-Heusler alloys with a large number of novel and desired properties are particularly appealing intermetallic compounds. Generally, these fascinating combinations take the form of ABC, where A denotes an element of the first main group; B represents a transition metal, noble metal, or rare earth element; and C represents an *sp*-valent element. Owing to promising potential applications in thermoelectricity [1], multifunctional materials [2, 3], topological devices [4–6], piezoelectrics [7], photoactivity [8–10], and optoelectronics [11, 12], the alloys have aroused increasing experimental and theoretical attention since the Heusler alloys were first reported by F. Heusler *et al.* in 1903.

Numerous experimental and theoretical studies have already been carried out. Most of the studies have focused on electronic, thermoelectronic, transport, magnetic, and piezoelectric properties of the alloys [3, 12–14]. As a member of this intriguing family, NaZnSb has also attracted increasing interest, because it is an outstanding candidate in the fields of topology [6], photoelectricity, magnetostriction, and thermoelectricity [15–19]. However, there are still some controversial issues, like the energy gap and phase transition. For example, Jaiganesh *et al.* [20] found that the energy gap of tetragonal NaZnSb was 0 eV and the pressure of the phase transition from the tetragonal structure to the cubic phase was 51.6 GPa using the tight-binding linear muffin-tin orbital (TB-LMTO) method in the atomic spheres approximation (ASA) consisting of the local density approximation (LDA) and the von Barth–Hedin scheme. Bennett *et al.* [2] reported that the energy gap of tetragonal NaZnSb was determined to be 0.54 eV by the projector augmented-wave method in the ABINIT package within the LDA. Recently, Charifi *et al.* [21] discovered that the pressure of the phase transition from the tetragonal structure to the cubic phase was 0.28 GPa using the full-potential linear augmented plane wave (FP-LAPW)

method and pseudopotential plane wave method implemented respectively by WIEN2K and the Quantum-Espresso (QE) package within the LDA. In addition, Reshak *et al.* [18, 19] investigated the electronic, thermodynamical, and optical properties of the tetragonal NaZnSb employing the state-of-the-art all-electron, full-potential linear augmented plane wave (FPLAPW) method within the modified Becke–Johnson potential (mBJ).

As mentioned above, there is a dearth of information about NaZnSb, especially in the fields of elasticity and thermodynamics. Furthermore, some discrepancies in the electronic properties and phase transition of NaZnSb have not been eliminated yet. Owing to the lack of related experiments, the theoretical values of the phase transition and energy gap are used as a reference. The original structures were fully optimized to obtain accurate results. Regarding the phase transition, we also take the effects of the Van der Waals interactions into consideration. Since the generalized gradient approximation and local density approximation possess rather simple forms and always underestimate the energy gap, the hybrid functional B3LYP is adopted to explore the energy gap of the NaZnSb in our work, which employs Becke's three-parameter functional and the Lee-Yang-Parr correlation functional. Moreover, the phase transformation of NaZnSb has rarely been investigated to date. The structural, mechanical, electronic, and bonding properties are important, since they can offer a deep insight into the inner properties of a material. For example, phase transformation is a ubiquitous and critical phenomenon in nature. Furthermore, it is an encouraging field full of opportunities and challenges. As the pressure or temperature varies, many materials undergo phase transformation. Generally, evolution of universes, syntheses of multifunctional devices, design of weapons, and laser fusion are all closely tied to phase transitions at high pressure and high temperature. It is noteworthy that remarkable changes in physical and chemical properties are often caused by phase transitions. In summary, the phase transformation of materials plays an important role in basic research, industries, national defense, and other areas. To provide a complementary study to both experimental and theoretical studies, we use the first-principles density functional theory (DFT) [22] method to systematically explore the structural, elastic, thermodynamical, electronic, and bonding properties and phase transition of NaZnSb.

The article is arranged as follows. In Section 2, the theoretical method and computation details are presented in detail. The results and discussion are presented in Section 3. Finally, we draw our conclusions in the last section.

2 Theoretical methods and computation details

2.1 Total energy electronic structure calculations

Based on DFT, we used the Cambridge Serial Total Energy Package (CASTEP) program [23] to probe the structural, mechanical, electronic, and bonding properties and phase transition of NaZnSb. Specifically, the exchange and correlation potentials were treated within both the generalized gradient approximation (GGA) [24] of Perdew-Burke-Ernzerhof (PBE) [25] and the local density approximation (LDA) [26] in the scheme of Ceperley-Alder [27] parametrized by Perdew and Zunger (CA-PZ) [28]. The non-local ultrasoft pseudopotentials introduced by Vanderbilt [29] were employed for the ion-electron interactions. Subsequently, pseudo-atomic calculations were implemented for Na-$2s^2 2p^6 3s^1$, Zn-$3d^{10} 4s^2$, and Sb-$5s^2 5p^3$. With the aim of producing accurate results, the electronic wave functions were expanded in a plane-wave basis set with an energy cut-off of 900 eV, and the K-space integrations for the tetragonal and cubic structures were carried out using $17 \times 17 \times 10$ and $19 \times 19 \times 19$ Monkhorst–Pack meshes [30] in the first Brillouin zone, respectively. The self-consistent convergence of the total energy is 5.0×10^{-7} eV/atom. With regard to full geometry optimization, the Brodyden–Fletcher–Goldfarb–Shanno (BFGS) minimization scheme [31] was adopted at different applied pressures. To guarantee the precision of the elastic constants, we employed a $19 \times 19 \times 11$ Monkhorst-Pack k mesh in the self-consistent calculations, which makes the tolerance of the difference in total energy less than 5×10^{-6} eV/atom and calculates the maximum magnitudes of the Hellmann-Feynman force, stress, and displacement to within 0.01 eV/Å, 0.02 GPa, and 5×10^{-4} Å, respectively. In addition, the hybrid functional B3LYP was used to accurately calculate the electronic band structures of tetragonal NaZnSb. The minor nature of the influence on the calculated results obtained by a set of more precise convergence tests suggests that these parameters are enough to guarantee reasonable results.

2.2 Elastic properties

For small strains, the elastic stiffness tensors at hydrostatic pressures are related to the stress and strain tensor, obeying Hooke's law. Generally, the elastic constant C_{ijkl} is calculated via the stress-strain curve or ensemble

averages of the fluctuations in stress. Here, the elastic constants were calculated by the former method. C_{ijkl} with respect to the finite strain is given by [32]

$$C_{ijkl} = \left(\frac{\partial \sigma_{ij}(\chi)}{\partial e_{kl}}\right)_{\mathrm{X}}, \tag{1}$$

in which σ_{ij}, e_{kl}, X, and χ represent the applied stress, Eulerian strain tensors, and coordinates before and after the deformation, respectively. As for the isotropic stress, we obtained

$$C_{ijkl} = c_{ijkl} + \frac{p}{2}(2\delta_{ij}\delta_{kl} - \delta_{il}\delta_{jk} - \delta_{ik}\delta_{jl}), \tag{2}$$

$$c_{ijkl} = \left(\frac{1}{V(\chi)}\frac{\partial^2 E(\chi)}{\partial e_{ij}\partial e_{kl}}\right)_{\mathrm{X}}, \tag{3}$$

where C_{ijkl} is the second-order derivative with respect to the infinitesimal (Eulerian) strain and δ represents the finite strain. In general, the fourth-rank tensor C has 21 non-zero independent components, because the stress and strain tensors are symmetric. Nevertheless, this number is greatly reduced when the symmetry of a crystal is considered. For a tetragonal crystal, the components are reduced to six, i.e., C_{11}, C_{33}, C_{44}, C_{66}, C_{12}, and C_{13}, which can be obtained by computing the stress generated by a small strain in an optimized unit cell [33]. In practice, six different strains are taken respectively to calculate the total energies, and the maximum strain amplitude is set to values from –0.003 to 0.003 in steps of 0.001.

Besides the elastic constants, the bulk modulus B is another significant physical quantity to use in depicting the contraction of a material when pressure is applied, while the shear modulus G reflects the resistance of an object to shear deformation. According to the Voigt and Reuss schemes [34], they are calculated using the available C_{ijkl} at hydrostatic pressures. In the Voigt scheme, B_V and G_V can be written as

$$B_V = \frac{2(C_{11}+C_{12})+C_{33}+4C_{13}}{9}, \tag{4}$$

$$G_V = \frac{2C_{11}-C_{12}+C_{33}-2C_{13}+6C_{44}+3C_{66}}{15}; \tag{5}$$

while in the Reuss scheme, B_R and G_R take the forms

$$B_R = \frac{(C_{11}+C_{12})C_{33}-2C_{13}^2}{C_{11}+C_{12}+2C_{33}-4C_{13}}, \tag{6}$$

$$G_R = 15/\{18B_V/[(C_{11}+C_{12})C_{33}-2C_{13}^2] + 6/(C_{11}-C_{12}) + 6/C_{44} + 3/C_{66}\}. \tag{7}$$

Hill [35] proved that the Voigt and Reuss equations denote the upper and lower limits, respectively. As a result, B and G can be expressed in terms of

$$B = \frac{1}{2}(B_R + B_V), \tag{8}$$

$$G = \frac{1}{2}(G_R + G_V), \tag{9}$$

where B_R, B_V, G_R, and G_V stand for the Reuss bulk modulus, Voigt bulk modulus, Reuss shear modulus, and Voigt shear modulus, respectively.

2.3 Thermodynamics properties

Using the Gibbs program, the quasi-harmonic Debye model [36] was used to explore the thermodynamic properties under different pressures and temperatures. In this model, the phonon effect was considered and the non-equilibrium Gibbs function $G^*(V;P,T)$ takes the form

$$G^*(V;P,T) = E(V) + PV + A_{Vib}(\Theta(V);T), \tag{10}$$

with $E(V)$ representing the total energy per unit cell, PV representing the constant hydrostatic pressure condition, $\Theta(V)$ corresponding to the Debye temperature, and A_{Vib} denoting the vibrational Helmholtz free energy, which can be written as [37]

$$A_{Vib}(\Theta;T) = nk_{\mathrm{B}}T\left[\frac{9\Theta}{8T} + 3\ln(1-\mathrm{e}^{-\Theta/T}) - D(\Theta/T)\right], \tag{11}$$

where $D(\Theta/T)$ represents the Debye integral, n denotes the number of atoms per formula unit, and K_B stands for the Boltzmann constant. For an isotropic solid, Θ is written as

$$\Theta = \frac{\hbar}{k_{\mathrm{B}}}(6\pi^2 V^{1/2} n)^{1/3} f(\sigma)\sqrt{\frac{B_S}{M}}, \tag{12}$$

where M stands for the molecular mass per formula unit, σ represents the Poisson ratio, $f(\sigma)$ is written in Ref. 38 as

$$f(\sigma) = \left\{3\left[2\left(\frac{2+2\sigma}{3-6\sigma}\right)^{3/2} + \left(\frac{1+\sigma}{3-3\sigma}\right)^{3/2}\right]^{-1}\right\}^{1/3}, \tag{13}$$

and B_s denotes the adiabatic bulk modulus, which is approximated by the static compressibility taking the form of [39]

$$B_S \cong B(V) = V\left\{\frac{\mathrm{d}^2 E(V)}{\mathrm{d}V^2}\right\}. \tag{14}$$

Consequently, the non-equilibrium Gibbs function $G^*(V;P,T)$ can be minimized with respect to the volume V:

$$\left(\frac{\partial G^*(V;P,T)}{\partial V}\right)_{P,T} = 0. \tag{15}$$

By solving Eq. (15), we obtain the thermal equation of state. Further, the isothermal bulk modulus B_T, the thermal expansion coefficient α, and the heat capacity C_V are respectively represented as

$$B_T(P,T) = V\left(\frac{\partial^2 G^*(V;P,T)}{\partial V^2}\right)_{P,T}, \tag{16}$$

$$\alpha = \frac{\gamma C_V}{B_T V}, \tag{17}$$

$$C_V = 3nk_{\mathrm{B}}\left[4D(\Theta/T) - \frac{3\Theta/T}{\mathrm{e}^{\Theta/T}-1}\right], \tag{18}$$

in which γ is the Grüneisen parameter expressed in terms of

$$\gamma = -\frac{\mathrm{d}\ln\Theta(V)}{\mathrm{d}\ln V}. \tag{19}$$

3 Results and discussion

3.1 Structural properties and phase transition

To understand the mechanical and electronic properties, it is essential to clarify the structures of NaZnSb. The previous studies on NaZnSb [3, 20, 21, 40, 41] have proposed tetragonal and face centered cubic (fcc) phases as possible structures. The foregoing texts give some details of the structures mentioned above. For example, the tetragonal phase with a space group of $P4/nmm$ is the ground state, while the fcc MgAgAs-type structures are its metastable states, which have the space group of $F\overline{4}3m$ [42]. Specifically, the tetragonal and cubic structures are illustrated in Fig. 1.

With the view of ascertaining the structural stability, the total energies in different phases were calculated using the CASTEP program within the framework of GGA rather than LDA, for the results calculated by GGA agree better with the available experimental data [41] and other theoretical results [2, 3, 6, 12, 20, 21, 40] displayed in Table 1 than do those by LDA. As displayed in Table 1, the computed structural parameters are excellently consistent with experimental values, with the overestimation of lattice constants characteristic of GGA calculations about as large as 0.2% for a and c, indicating the reliability of our calculations. As a result, the following calculations of the structural, mechanical,

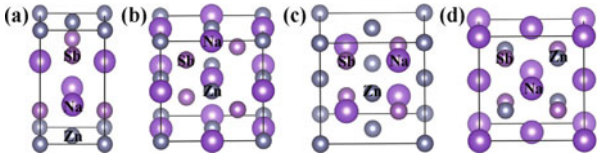

Fig. 1 Four structures: **(a)** Tetragonal structure, **(b)** Cubic α-phase, **(c)** Cubic β-phase, **(d)** Cubic γ-phase.

Table 1 Equilibrium lattice constants a_0 and c_0 (Å), the ratio of c_0/a_0, bulk modulus B_0 (GPa) and its first pressure derivative B_0' of NaZnSb at 0 GPa and 0 K, in comparison with the available values.

structure		a_0	c_0	c_0/a_0	B_0	B_0'
Tetragonal	Present	4.451	7.505	1.6862	38.48	4.62
	Expt. [41]	4.442	7.489	1.686		
	Cal. [2]	4.56	7.33	1.6075		
	Cal. [3]	4.558	7.332	1.6086		
	Cal. [20]	4.365	7.363	1.6868	95.34	
	Cal. [21]	4.46	7.488	1.679	38.41	4.78
	Cal. [40]	4.442	7.492	1.6866		
α-cubic	Present	6.74			33.69	4.39
	Cal. [12]	6.763				
	Cal. [20]	6.277			86.91	
	Cal. [21]	6.767			33.8	4.33
β-cubic	Present	6.582			38.15	4.69
	Cal. [21]	6.568			38.7	4.71
γ-cubic	Present	6.764			27.33	4.71
	Cal. [21]	6.753			27.5	4.66

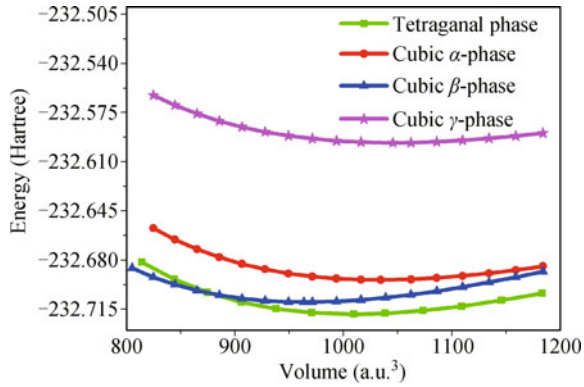

Fig. 2 The total energies versus primitive cell volume at 0 K for the tetragonal and cubic NaZnSb.

electronic, and bonding properties were also carried out by GGA. The calculated results generally show a good agreement with aforementioned researches. Fig. 2 shows that the tetragonal phase is the most stable structure at 0 GPa and 0 K.

To further investigate the ground state of NaZnSb, we probed the phase transition between the tetragonal and cubic structures. As is known, the pressure of the phase transition at 0 K can be obtained from the usual condition of equal enthalpy ($H = E + PV$). In the case of NaZnSb, the variations of the enthalpies with pressures at 0 K are plotted in Fig. 3.

Obviously, the intersection of enthalpy-pressure curves between the tetragonal and cubic structures indicates that the value of the transition pressure from the tetragonal structure to the cubic beta phase is about 5.96 GPa. Therefore, the tetragonal structure is the most stable

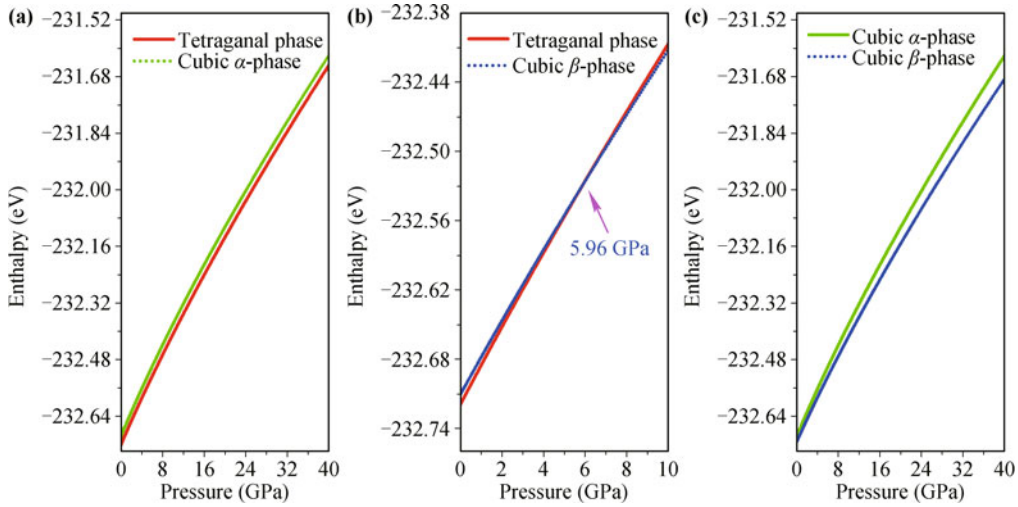

Fig. 3 The calculated enthalpy versus pressure at 0 K: **(a)** for the tetragonal structure and cubic alpha phase, **(b)** for the tetragonal structure and cubic beta phase, **(c)** for cubic alpha phase and cubic beta phase.

state at applied pressures ranging from 0 to 5.96 GPa, which agrees well with the conclusion drawn by the analysis of the structures above. Though our measurement of the pressure of the phase transition is between 0.28 [21] and 59.6 GPa [20], further experimental and theoretical studies are needed for verification. Owing to the dearth of experimental data, we calculated the Gibbs free energy of tetragonal and cubic structures at 300 K for comparison. Based on the criterion of equal Gibbs free energy, we ascertained the pressure of the phase transition from the tetragonal structure to cubic beta phase at 300 K, which is about 5.17 GPa. This shows that the value of the phase transition pressure decreases with increasing temperature. Surprisingly, there is no phase transition between the tetragonal and cubic alpha structures in the studied pressure range, which is in contrast to their analogous compounds. Unfortunately, there are no experimental data for comparison; hence, further investigations need to be carried out. Consequently, the following calculations of mechanical, electronic, and bonding properties were focused on the tetragonal structure. The calculated E–V data at 0 K were fitted to the third-order Birch–Murnaghan equation of state (EOS) [41] to gain the theoretical equilibrium volume V_0 and the bulk modulus B_0 and its pressure derivative B_0', which are also listed in Table 1. From Table 1, it can be clearly found that the values of B_0 and B_0' are in line with those of Ref. 21 but are different from the data of Ref. 20. In other words, the bulk modulus and its pressure derivative are still unresolved.

With the purpose of further understanding the physical changes of the tetragonal structure, we illustrate the variations of the volume ratio V/V_0 with pressure and temperature in Fig. 4, where V_0 represents the equilibrium primitive volume at 0 K.

It is clearly seen that the volume ratio declines with rising pressure at a given temperature. In addition, it also exhibits a downward trend with increasing temperature. Furthermore, the values of V/V_0 at higher temperature are smaller than those in the lower temperature region at the same pressure. It is noteworthy that slopes of the V/V_0–P curves decrease monotonically with increasing pressure, and this fact implies that the compressibility of NaZnSb in the tetragonal phase becomes smaller and smaller. Since there is no available experimental or theoretical data, we hope that our results will serve as a complement.

3.2 Elastic properties at 0 K

Elastic properties are crucial to understanding mechanical strength, bonding properties between adjacent atomic planes, anisotropic character, and structural

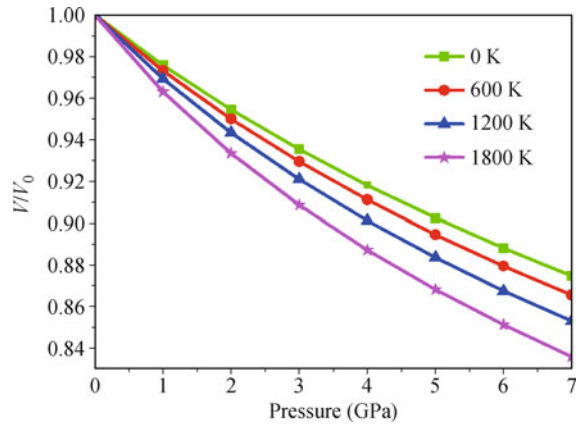

Fig. 4 The volume ratio V/V_0 versus pressure for the tetragonal NaZnSb.

stability [43]. For instance, C_{ijkl} plays an important role in practical applications such as anisotropy, internal strain, thermoelastic stress, structural stability, and load deflection. Pressure is also an important factor in determining the physical properties. For a tetragonal crystal, the elastic constants $C_{11}$and C_{33} represent elasticity in length, while C_{44}, C_{66}, C_{12}, and C_{13} characterize elasticity in shape. The independent elastic constants of the tetragonal phase, C_{11}, C_{33}, C_{44}, C_{66}, C_{12}, and C_{13}, are listed in Table 2. The elastic constants as functions of the hydrostatic pressure are also shown in Fig. 5.

It is a pity that there are no related experimental or theoretical data for the tetragonal NaZnSb up to now. To test the reliability of our calculational methods, we also calculated the elastic constants of NaZnSb in the cubic phase. Our values of C_{11}, C_{12}, and C_{44} are 58.40836, 22.2914, and 27.39519 GPa, respectively, which agree well with those (57.9957, 22.2666, and 28.7287 GPa, respectively) of Ref. 16. In other words, the method used in the present paper is reliable and our calculated elastic constants are accurate. As illustrated in Fig. 5, the elastic constants exhibit an upward trend as pressure grows. Moreover, C_{11}, C_{33}, C_{12}, and C_{13} are susceptible to pressure, while C_{44} and C_{66} remain almost unchanged with increasing pressure. In addition, $C_{11} = C_{22}$ is larger than C_{33} in the whole range of the studied pressure, which indicates that the c-axis is easier to shrink and has a larger strain under normal stress with the same value; in other words, the atomic bonds along the $\langle 100 \rangle$ and $\langle 010 \rangle$ directions are stronger than those along the $\langle 001 \rangle$ direction. As for the shear modulus, the value of C_{13} is always larger than that of C_{66}, which reveals that the shear deformation corresponding to C_{66} more easily occurs when the shear stresses are applied on the vertical $\{1\ 0\ 0\}$ plane along the horizontal $\langle 100 \rangle$ direction. In a sense, these distinct differences between the elastic constants also imply the mechanical anisotropy of NaZnSb. It is worth noting that C_{33} manifests a change from an upward trend to a downward one in the pressure range of 6.0–7.0 GPa, which is related to the phase transition.

Table 2 Elastic constants C_{ij} (GPa), bulk modulus B (GPa) and shear modulus G (GPa) versus pressure P (GPa) at 0 K for the tetragonal NaZnSb.

P	C_{11}	C_{33}	C_{44}	C_{66}	C_{12}	C_{13}	B	G
0.0	70.594	57.216	10.278	6.081	18.573	19.600	37.057	14.041
1.0	79.768	64.629	11.364	8.034	21.351	23.307	41.729	15.632
2.0	86.703	72.059	12.256	9.920	23.585	26.787	46.223	17.087
3.0	93.720	77.553	12.965	11.685	26.831	30.446	50.480	18.409
4.0	100.860	83.740	13.673	13.334	29.575	33.635	54.700	19.605
5.0	106.685	90.396	14.318	15.171	32.225	37.799	58.300	20.522
6.0	114.218	96.467	14.700	17.109	36.270	40.852	62.388	21.503
7.0	120.239	95.369	15.135	18.988	39.339	43.638	65.085	22.199

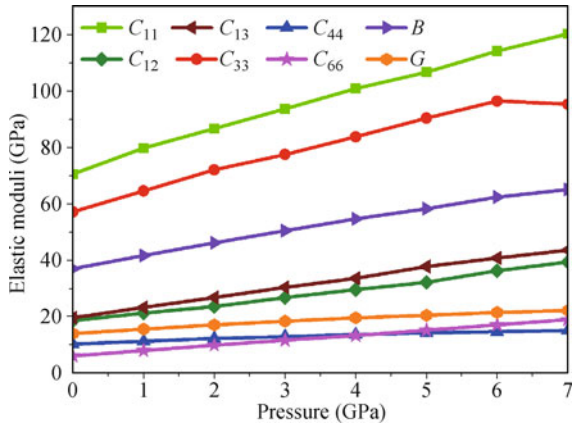

Fig. 5 The elastic constants and modulus versus pressure at 0 K for the tetragonal NaZnSb.

For the purpose of further probing the stability of NaZnSb, the mechanical stability of tetragonal crystals is employed, which is as follows [34]:

$$\begin{aligned} &C_{11} > 0, \quad C_{33} > 0, \quad C_{44} > 0, \quad C_{66} > 0, \\ &C_{11} - C_{12} > 0, \quad C_{11} + C_{33} - 2C_{13} > 0, \\ &2(C_{11} + C_{12}) + C_{33} + 4C_{13} > 0. \end{aligned} \tag{20}$$

These criteria are valid only for the special case of 0 GPa. In the case of the tetragonal phase at hydrostatic pressures, the general elastic stability criteria are expressed as follows [44]:

$$\begin{aligned} &\tilde{C}_{11} > 0, \quad \tilde{C}_{33} > 0, \quad \tilde{C}_{44} > 0, \quad \tilde{C}_{66} > 0, \\ &\tilde{C}_{11} - \tilde{C}_{12} > 0, \quad \tilde{C}_{11} + \tilde{C}_{33} - 2\tilde{C}_{13} > 0, \\ &2\tilde{C}_{11} + 2\tilde{C}_{12} + \tilde{C}_{33} + 4\tilde{C}_{13} > 0, \end{aligned} \tag{21}$$

where the elastic stiffness coefficient $\tilde{C}_{ij}$ is related to C_{ij} by

$$\begin{aligned} &\tilde{C}_{\alpha\alpha} = C_{\alpha\alpha} - P \ (\alpha = 1, 3, 4, 6), \quad \tilde{C}_{12} = C_{12} + P, \\ &\tilde{C}_{13} = C_{13} + P. \end{aligned} \tag{22}$$

The mechanical properties of materials vary with the occurrence of phase transitions. By studying the elastic constants, we have found that they meet all of the elastic stability criteria at external isotropic pressures up to 5.96 GPa, which implies that NaZnSb in the tetragonal phase is mechanically stable.

It should be noted that the strain rate and thermal activation are important factors in affecting structural stability under the influence of temperature and pressure, especially when plastic deformation and trigger reactions take place [45, 46]. Consequently, the criteria of stability mentioned above need to be perfected by taking strain rate and thermal activation into account, which needs persistent research.

Since the elastic anisotropic behaviors play important

roles in engineering science and crystal physics, it is essential to further explore them. For example, the shear anisotropic factors indicate the degree of anisotropy in the bonding between corresponding atoms in different planes. Specifically, the shear anisotropic factor for the {1 0 0} plane between the ⟨011⟩ and ⟨010⟩ directions is defined as follows:

$$A_1 = \frac{4C_{44}}{C_{11} + C_{33} - 2C_{13}}. \tag{23a}$$

For the {0 1 0} plane between the ⟨101⟩ and ⟨001⟩ directions, it takes the form of

$$A_2 = \frac{4C_{55}}{C_{22} + C_{33} - 2C_{23}}. \tag{23b}$$

And, for the {0 0 1} plane between the ⟨110⟩ and ⟨010⟩ directions, it is expressed as

$$A_3 = \frac{4C_{66}}{C_{11} + C_{22} - 2C_{12}}. \tag{23c}$$

In the case of an isotropic crystal, A_1, A_2, and A_3 should equate to one; any value smaller or greater than one indicates the degree of elastic anisotropy [47]. We find that the values of the shear anisotropic factors are all less than one. Specifically, the value of A_3 is less than those of A_1 and A_2, which indicates the degree of the anisotropy in the {0 0 1} plane is more serious than those of the {1 0 0} and {0 1 0} planes. Furthermore, each of the shear anisotropic factors manifests an upward trend when the pressure increases. It is noteworthy that a change from an upward trend to a downward one is observed in the pressure range of 5.0–7.0 GPa, which is related to the phase transition.

As is known, elastic moduli play important roles in science studies and engineering applications. Generally, Θ_D denotes the resistance to fracture, while γ represents the resistance to plastic deformation. Hardness can be directly evaluated for the strongly covalent materials [48]. With regard to the partially covalent transition metal–based hard materials, α and γ can be used to measure the hardness indirectly. Excitingly, we can obtain α and γ using the calculated elastic constants, which were listed in Table 2 and illustrated in Fig. 5. Obviously, both γ and γ at 0 K exhibit a moderate upward trend when the pressure increases from 0 to 7.0 GPa, which indicates that the compressibility of NaZnSb becomes more and more difficult with growing pressure, which is in line with the conclusion of V/V_0. With the view of measuring the degree of ductility of materials effectively, a ratio of bulk versus shear modulus, B/G, was reported by Pugh [49]. In general, crystals becomes more and more ductile with the increase of B/G. Specifically, the material is ductile when the values of B/G are larger than 1.75; otherwise it behaves in a brittle manner. Regarding NaZnSb at 0 GPa and 0 K, the value of B/G is 2.639, suggesting that it is ductile in nature. As pressure increases, the ratio of B/G changes from 2.639 to 2.932, which indicates that NaZnSb grows more and more ductile.

3.3 Thermodynamic properties

Great potentials of the thermodynamic properties in material science spurred us to probe the Grüneisen parameter γ, thermal expansivity α, heat capacity C_V, Debye temperature Θ_D, and entropy S, which are listed in Table 3 and displayed in Figs. 6–10, respectively.

As pressure increases from 0 to 7.0 GPa, the values of γ diminish by 6.77%, 7.95%, 9.80%, and 12.6%, and α also decreases by 0.00%, 40.7%, 45.8%, and 53.6% at 0, 600, 1200, and 1800 K, respectively.

As illustrated in Figs. 6 and 7, both γ and α manifest a similar downward trend with increasing pressure. In addition, they increase when temperature increases. In particular, γ decreases sharply with increasing pressure at a constant temperature, whereas γ increases markedly with the increase of temperature at a given pressure. Moreover, γ decreases with the increase of pressure more quickly in the high-temperature region than at lower temperature. However, it rises with increasing temperature more slowly at higher pressure than in the low-pressure area. For a given pressure, αrises exponentially in the low-temperature region and then tends to a linear increase with increasing temperature, since the anharmonic effect becomes weaker. Moreover, as the pressure increases, the amount of increase of α with increasing temperature becomes smaller, especially in the high-temperature area. At a constant temperature, α exhibits a trend clearly different from that at a fixed pressure. Owing to the reduction of the anharmonic effect in the high-temperature region, α decreases visibly and the influence of pressure diminishes gradually when the pressure increases.

In addition, the heat capacity C_V can provide some crucial information about heat transmission processes and vibrational properties, which reveals the inherent characterization of materials. From Table 3, it is worth pointing out that when the applied pressure grows from 0 to 6.0 GPa, the heat capacity C_V lessens by 0.000%, 0.669%, 0.172%, and 0.079% at 0, 600, 1200, and 1800 K, respectively.

From Fig. 8, we can clearly see that C_V exhibits an upward trend with increasing temperature, similar to γ

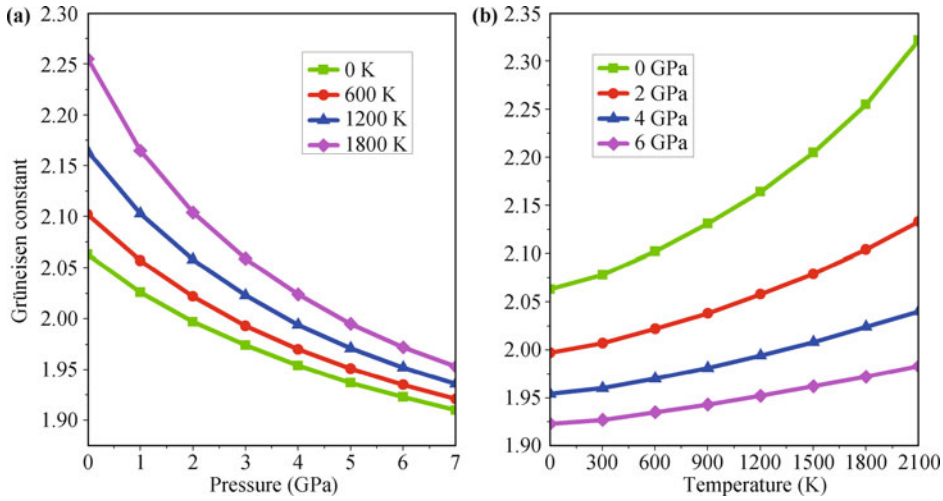

Fig. 6 Grüneisen parameter γ versus pressure **(a)** and temperature **(b)** for the tetragonal NaZnSb.

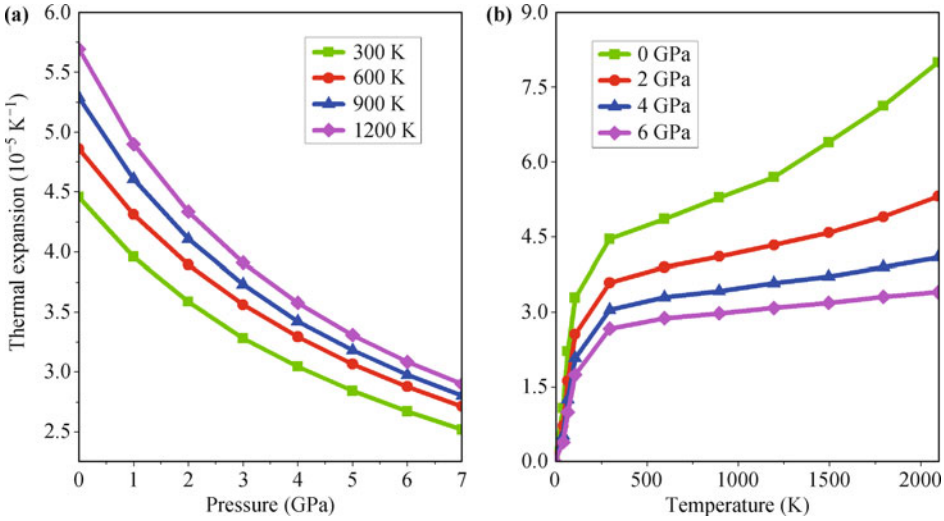

Fig. 7 Thermodynamic expansivity α versus pressure **(a)** and temperature **(b)** for the tetragonal NaZnSb.

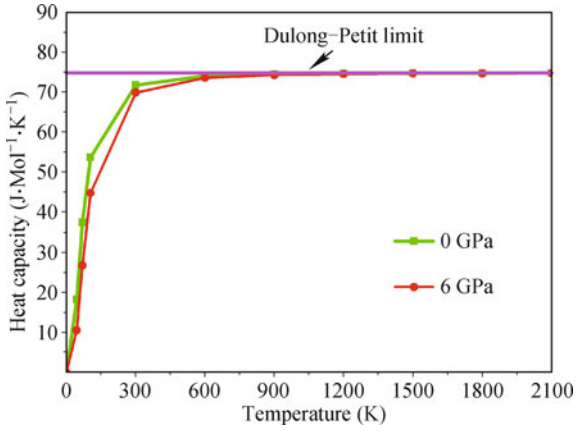

Fig. 8 Teat capacity C_V versus temperature for the tetragonal NaZnSb.

and α. It is noteworthy that the impact on C_V derived from temperature is far greater than that of pressure in the low-temperature region. Specifically, at a constant pressure, C_V is greatly dependent on temperature when the temperature is below 300 K; the anharmonic approximation of the Debye model is considered in the calculation. On the other hand, in the high-temperature area, the anharmonic effect on C_V is suppressed and the enhancement of the heat capacity becomes smaller and smaller, finally tending to zero. In other words, when the temperature continually increases, C_V obeys the Debye law and approaches the Dulong–Petit limit.

It is known that the Debye temperature Θ_D is closely related to vibrations of lattice, elastic constants, melting temperature, specific heat, and so on. Hence, we probe its related behaviors. When the temperature is below the Debye temperature Θ_D, the vibrational excitations of the lattice are derived mainly from acoustic vibrations, and

Table 3 Grüneisen constant γ, thermal expansion coefficient $\alpha(10^{-5}\ \mathrm{K}^{-1})$, heat capacity C_V ($\mathrm{J{\cdot}mol^{-1}{\cdot}K^{-1}}$), Debye temperature Θ_D (K) and entropy S ($\mathrm{J{\cdot}K^{-1}}$) at different pressures and temperatures for the tetragonal NaZnSb.

T (K)	P (GPa)	0	2	4	6
0	γ	2.063	1.997	1.954	1.923
	α	0	0	0	0
	C_V	0	0	0	0
	Θ_D	281.710	309.640	334.330	356.620
	S	0	0	0	0
300	γ	2.078	2.007	1.960	1.927
	α	4.456	3.586	3.044	2.670
	C_V	71.751	71.100	70.485	69.897
	Θ_D	276.270	305.060	330.260	352.970
	S	107.502	100.422	94.802	90.134
600	γ	2.102	2.022	1.970	1.935
	α	4.858	3.893	3.293	2.879
	C_V	74.088	73.914	73.750	73.592
	Θ_D	268.300	298.210	324.110	347.310
	S	160.372	152.550	146.402	141.309
900	γ	2.131	2.038	1.981	1.943
	α	5.287	4.106	3.422	2.976
	C_V	74.520	74.440	74.366	74.295
	Θ_D	259.820	291.190	317.980	341.430
	S	192.899	184.411	177.860	172.573
1200	γ	2.164	2.058	1.994	1.952
	α	5.692	4.335	3.577	3.085
	C_V	74.667	74.622	74.580	74.539
	Θ_D	250.820	283.600	311.170	335.520
	S	216.991	207.822	200.902	195.285
1500	γ	2.205	2.079	2.008	1.962
	α	6.394	4.584	3.713	3.185
	C_V	74.734	74.704	74.677	74.651
	Θ_D	241.140	276.080	304.390	329.300
	S	236.601	226.489	219.199	213.326
1800	γ	2.255	2.104	2.024	1.972
	α	7.122	4.900	3.893	3.306
	C_V	74.769	74.748	74.729	74.710
	Θ_D	230.550	267.790	297.460	323.060
	S	253.589	242.392	234.540	228.371
2100	γ	2.322	2.133	2.040	1.983
	α	7.992	5.310	4.087	3.399
	C_V	74.790	74.774	74.759	74.745
	Θ_D	218.620	259.290	290.440	316.910
	S	269.090	256.328	247.848	241.326

the quantum mechanical effect is an important factor in tuning the thermodynamic properties. Nevertheless, it can be ignored when the temperature is above Θ_D. Specifically, the Debye temperature Θ_D increases by 26.6%, 29.4%, 33.8%, and 40.1% at 0, 600, 1200, and 1800 K, respectively.

As illustrated in Fig. 9, for a fixed pressure, the Debye temperature Θ_D decreases monotonically with increasing temperature, while it exhibits an upward tendency when the pressure increases, which indicates that the frequency of the acoustic vibrational excitations grows when the pressure increases. In addition, the effect of pressure on the Debye temperature Θ_D grows weak with the increase of temperature.

Last but not least, as displayed in Fig. 10, the entropy S is also affected by both pressure and temperature, and the impact of increasing pressure on tetragonal NaZnSb is the same as decreasing temperature. Moreover, the effect of temperature is greater than that of pressure. At a given temperature, the entropy decreases quickly with increasing pressure, while the entropy at lower temperature is less than that at higher temperature for a given pressure.

3.4 Electronic and bonding properties at 0 K

The band structures and density of states are vital for analyzing the physical properties of materials. As a result, we explore the band structures and density of states. First of all, we calculate the electronic band structures of tetragonal NaZnSb at 0 GPa and 5.96 GPa and then illustrate them along high-symmetry lines in Fig. 11.

As shown in Fig. 11, the profile of the band structures resembles those of Refs. 20 and 21, which are derived from the presence of two molecules per formula unit. In addition, the conduction band minimum (CBM) and valence band maximum (VBM) lie in the center of the Brillouin zone at 0 GPa and 0 K, leading to a band gap of about 0.41 eV. Furthermore, this is a direct-gap semiconductor, for the CBM and VBM are located at the same high-symmetry point G. This conclusion is consistent with those drawn respectively by Joseph *et al.* [2], Kacimi *et al.* [12], and the Reshak group [18,19], but inconsistent with the verdicts of Jaiganesh *et al.* [20], Charifi *et al.* [21], and Madsen [40], who considered NaZnSb to be a metal. Consequently, further theoretical and experimental studies are urgently needed. As pressure increases, the band gap of tetragonal NaZnSb becomes larger and larger, which shows that its semiconducting character is retained.

To further illuminate the nature of the electronic properties, we also investigate the total density of states (TDOS) and partial density of states (PDOS) at 0 and 5.96 GPa and demonstrate them in Fig. 12.

With the purpose of producing the smooth DOS picture, a 0.1 eV smearing of the energy levels is implemented. As shown in Fig. 12, the CBM is mainly contributed by the Sb-p orbital; simultaneously, it also includes a little contribution from the Zn-s and Na-p orbitals. The VBM consists of Na-p, Zn-p, and Sb-p states. Meanwhile, semiconducting behavior is also evident,

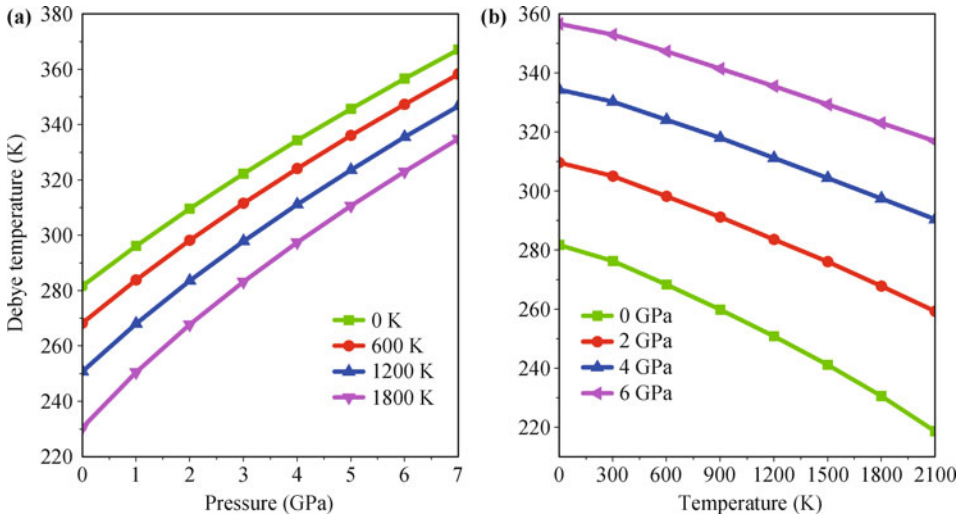

Fig. 9 Debye temperature Θ_D versus pressure **(a)** and temperature **(b)** for the tetragonal NaZnSb.

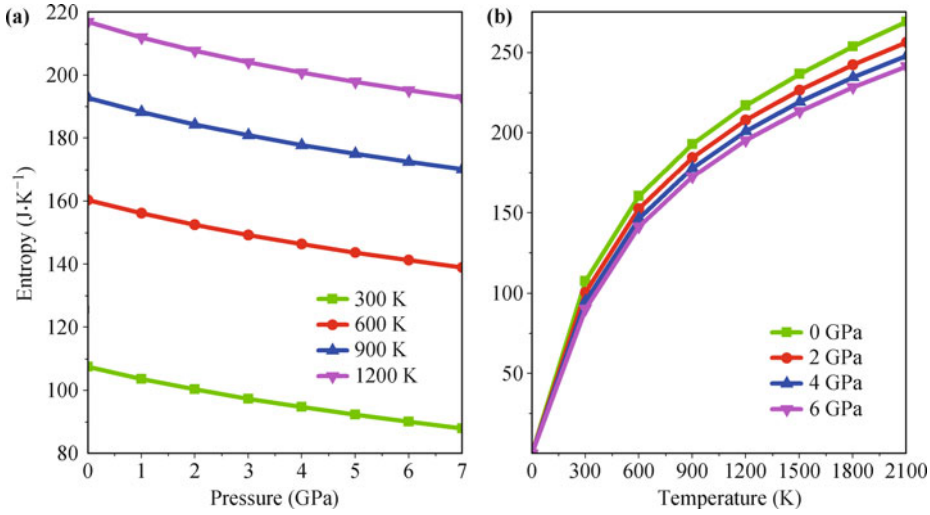

Fig. 10 Entropy S versus pressure **(a)** and temperature **(b)** for the tetragonal NaZnSb.

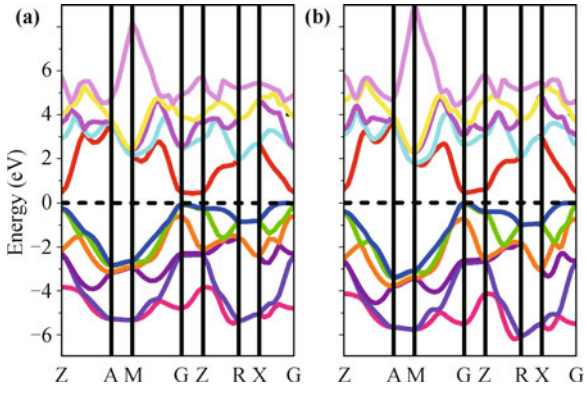

Fig. 11 Band structures for tetragonal NaZnSb at pressures of 0 **(a)** and 5.96 GPa **(b)**.

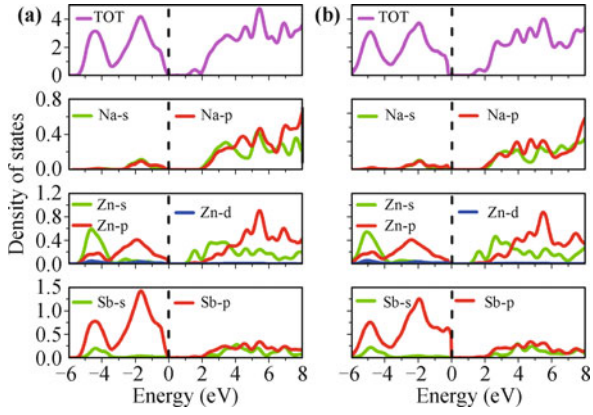

Fig. 12 Density of states for the tetragonal NaZnSb at pressures of 0 **(a)** and 5.96 GPa **(b)**.

because there is a band gap of about 0.40 eV at the Fermi level E_F. This conclusion is in good agreement with that of the band structures. Moreover, the peak in the energy range from –5 to –4 eV is mainly contributed by the s state of the Zn atom and the p state of the

Sb atom, while also containing a little contribution from the p orbital of the Zn atom and the s orbital of the Sb atom. It is noteworthy that there is a distinct hybridization between Zn $s$and Sb p in this energy region. Other hybridizations between Zn-p and Na-s states were also observed, which may cause strong covalent bonding between these atoms. In addition, there is the other distinct peak in the valence bands region, the dominant contribution to which comes from the p-like states of the Zn and Sb atoms. For the case of the conduction bands, there is no sharp peak except the one situated in the energy range 5.0 to 6.0 eV, which comes mainly from the p states of the Zn and Na atoms. When NaZnSb is compressed, the peaks of DOS in the valence bands have a tendency of shifting to lower energy and the values of the peaks become smaller. Take the p state of the Sb atom as an example: the two peaks are shifted from –4.42 and –1.67 eV to –4.91 eV and –1.98 eV, respectively, in the range of pressures from 0.0 to 5.96 GPa. As pressure increases, the valence bands tend to broaden and shift toward the lower-energy region, whereas the conduction bands transfer to the higher-energy region. It is understood that the overlap of the bands is increased and the corresponding hybridization is changed. Under external pressure, the inter-atomic spacing is expected to be decreased and the overlap of the wave functions also becomes stronger. Hence, there is an increment in the dispersion and bandwidth of the bands.

To inspect the bonding property, we make further investigations into the Mulliken overlap population [50] and electron density map of tetragonal NaZnSb. As a common rule, the Mulliken overlap population is an objective and quantitative criterion for assessing the covalent or ionic nature of bonds. It is well known that a negative value indicates an anti-bonding state and a zero value implies a perfect ionic bond, while a value increasingly greater than zero indicates an increasing degree of covalency [51]. Therefore, the technique for the projection of plane-wave states onto a localized basis set proposed by Segall *et al.* was used to calculate atomic charges and bond populations by means of Mulliken analysis. The Mulliken charges and overlap populations of NaZnSb in the tetragonal phase at 0 GPa and 0 K are presented in Table 4. The atomic populations in the table reveal that there are 0.72 electrons transferred from the Na atom to the Sb atom, but for Zn, the value is only 0.09, which indicates that the Na-Sb bond has more ionic character. The bond population of the Zn-Sb bond is 0.83, which is larger than that of the Na-Sb bond, implying that the covalent character of the former is more notable than the latter. To show it more visually, we have also plotted the charge density map of the {1 0 0} plane in Fig. 13.

Table 4 Charge transfers (e) and bond populations P (e) of the tetragonal NaZnSb at 0 Gpa and 0 K.

Species	s	p	d	Total	Charge	Band	P
Na	2.15	6.04	0	8.19	0.81	Na-Sb	0.09
Zn	0.72	1.40	9.97	12.09	–0.09	Na-Zn	–0.81
Sb	1.92	3.79	0	5.72	–0.72	Zn-Sb	0.83

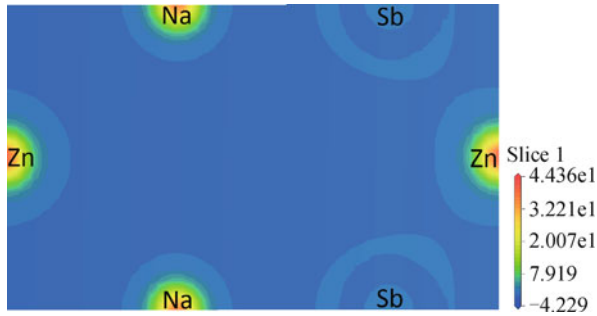

Fig. 13 Map of the Charge density in the (1 0 0) plane of the tetragonal NaZnSb at 0 GPa and 0 K.

Apparently, the charge density distribution between Zn and Sb is distinct, but that between Na and Sb is inconspicuous, conforming to our former analysis that there is more covalent character in the Zn–Sb bond.

4 Conclusions

We carried out a detailed exploration of structural, mechanical, electronic, and bonding properties, as well as phase transition, via first-principles density functional theory calculations. Our results indicated that the tetragonal phase is more stable than corresponding cubic structures in the pressure range from 0 to 5.96 GPa, i.e., the tetragonal phase is the ground state structure. It is worth noting that tetragonal-cubic (β) occurred at 5.96 GPa. Subsequently, the elastic properties of tetragonal NaZnSb were discussed. We also investigated the Grüneisen parameter, thermal expansivity, heat capacity, and Debye temperature for the first time. In addition, the electronic properties indicate that NaZnSb in the ground state exhibits a distinct semiconducting behavior. From the analysis of the bonding properties, we find that the Na-Sb bond shows an ionic behavior, while the Zn-Sb bond exhibits a covalent one.

Acknowledgements The authors would like to thank the support by the National Natural Science Foundation of China under Grant Nos. 11204192 and 11272293, the NSAF under Grant No. U1230201, the Defense Industrial Technology Development Program of China under Grant No. B1520110002, the National Key Laboratory Fund for Shock Wave and Detonation Physics Research of the China Academy of Engineering Physics under Grant No. 2012-Zhuan-08, and the Science and Technology Development

Foundation of China Academy of Engineering Physics under Grant Nos. 2012A0201007 and 2013B0101002. We also acknowledge the support for the computational resources by the State Key Laboratory of Polymer Materials Engineering of China in Sichuan University.

References

1. B. Balke, J. Barth, M. Schwall, G. H. Fecher, and C. Felser, An alternative approach to improve the thermoelectric properties of half-Heusler compounds, *J. Electron. Mater.* 40(5), 702 (2011)
2. J. W. Bennett, K. F. Garrity, K. M. Rabe, and D. Vanderbilt, Orthorhombic ABC semiconductors as antiferroelectrics, *Phys. Rev. Lett.* 110(1), 017603 (2013)
3. J. W. Bennett, K. F. Garrity, K. M. Rabe, and D. Vanderbilt, Hexagonal ABC semiconductors as ferroelectrics, *Phys. Rev. Lett.* 109(16), 167602 (2012)
4. S. Chadov, X. Qi, J. Kubler, G. H. Fecher, C. Felser, and S. C. Zhang, Tunable multifunctional topological insulators in ternary Heusler compounds, *Nat. Mater.* 9(7), 541 (2010)
5. H. Lin, A. Wray, Y. Xia, S. Xu, S. Jia, R. J. Cava, A. Bansil, and M. Z. Hasan, Half-Heusler ternary compounds as new multifunctional experimental platforms for topological quantum phenomena, *Nat. Mater.* 9(7), 546 (2010)
6. H. J. Zhang, S. Chadov, L. Müchler, B. Yan, X. L. Qi, J. Kübler, S. C. Zhang, and C. Felser, Topological insulators in ternary compounds with a honeycomb lattice, *Phys. Rev. Lett.* 106(15), 156402 (2011)
7. A. Roy, J. W. Bennett, K. M. Rabe, and D. Vanderbilt, Half-Heusler semiconductors as piezoelectrics, *Phys. Rev. Lett.* 109(3), 037602 (2012)
8. J. W. Bennett, I. Grinberg, and A. M. Rappe, New highly polar semiconductor ferroelectrics through d8 cation-O vacancy substitution into $PbTiO_3$: A theoretical study, *J. Am. Chem. Soc.* 130(51), 17409 (2008)
9. J. W. Bennett, I. Grinberg, P. K. Davies, and A. M. Rappe, Pb-free semiconductor ferroelectrics: A theoretical study of Pd-substituted $Ba(Ti_{1-x}Ce_x)O_3$ solid solutions, *Phys. Rev. B* 82(18), 184106 (2010)
10. G. Y. Gou, J. W. Bennett, H. Takenaka, and A. M. Rappe, Post density functional theoretical studies of highly polar semiconductive $Pb(Ti_{1-x}Ni_x)O_{3-x}$ solid solutions: Effects of cation arrangement on band gap, *Phys. Rev. B* 83(20), 205115 (2011)
11. D. Kieven, R. Klenk, S. Naghavi, C. Felser, and T. Gruhn, I-II-V half-Heusler compounds for optoelectronics: Ab initio calculations, *Phys. Rev. B* 81(7), 075208 (2010)
12. S. Kacimi, H. Mehnane, and A. Zaoui, I-II-V and I-III-IV half-Heusler compounds for optoelectronic applications: Comparative ab initio study, *J. Alloys Compd.* 587, 451 (2014)
13. M. S. Lee, F. P. Poudeu, and S. D. Mahanti, Electronic structure and thermoelectric properties of Sb-based semiconducting half-Heusler compounds, *Phys. Rev. B* 83(8), 085204 (2011)
14. A. F. May, E. S. Toberer, and G. J. Snyder, Transport properties of the layered Zintl compound $SrZnSb_2$, *J. Appl. Phys.* 106(1), 013706 (2009)
15. D. M. Wood, A. Zunger, and R. de Groot, Electronic structure of filled tetrahedral semiconductors, *Phys. Rev. B* 31(4), 2570 (1985)
16. R. Bacewicz and T. F. Ciszek, Preparation and characterization of some AIBIICIII type semiconductors, *Appl. Phys. Lett.* 52(14), 1150 (1988)
17. A. Beleanu, M. Mondeshki, Q. Juan, F. Casper, C. Felser, and F. Porcher, Systematical, experimental investigations on LiMgZ (Z = P, As, Sb) wide band gap semiconductors, *J. Phys. D* 44(47), 475302 (2011)
18. A. H. Reshak and S. Auluck, Thermoelectric properties of Nowotny–Juza NaZnX (X = P, As and Sb) compounds, *Comput. Mater. Sci.* 96, 90 (2015)
19. A. H. Reshak, Nowotny–Juza NaZnX (X = P, As and Sb) as photovoltaic materials, *Sol. Energy* 115, 430 (2015)
20. G. Jaiganesh, T. Merita Anto Britto, R. D. Eithiraj, and G. Kalpana, Electronic and structural properties of NaZnX (X = P, As, Sb): An ab initio study, *J. Phys.: Condens. Matter* 20(8), 085220 (2008)
21. Z. Charifi, H. Baaziz, S. Noui, Ş. Uğur, G. Uğur, A. İyigör, A. Candan, and Y. AlDouri, Phase transition of Nowotny–Juza NaZnX (X = P, As and Sb) compounds at high pressure: Theoretical investigation of structural, electronic and vibrational properties, *Comput. Mater. Sci.* 87, 187 (2014)
22. W. Kohn and L. Sham, Self-consistent equations including exchange and correlation effects, *Phys. Rev.* 140(4A), A1133 (1965)
23. B. Zhu, Y. Cheng, Z. W. Niu, M. Zhou, and M. Gong, LDA+U calculation of structural and thermodynamic properties of Ce_2O_3, *Front. Phys.* 9(4), 483 (2014)
24. B. Hammer, L. B. Hansen, and J. K. Norskov, Improved adsorption energetics within density-functional theory using revised Perdew–Burke–Ernzerhof functionals, *Phys. Rev. B* 59(11), 7413 (1999)
25. J. P. Perdew, K. Burke, and M. Ernzerhof, Generalized gradient approximation made simple, *Phys. Rev. Lett.* 77(18), 3865 (1996)
26. S. H. Vosko, L. Wilk, and M. Nusair, Accurate spin-dependent electron liquid correlation energies for local spin density calculations: A critical analysis, *Can. J. Phys.* 58(8), 1200 (1980)
27. D. M. Ceperley and B. J. Alder, Ground state of the electron gas by a stochastic method, *Phys. Rev. Lett.* 45(7), 566 (1980)
28. J. Perdew and A. Zunger, Self-interaction correction to density-functional approximations for many-electron systems, *Phys. Rev. B* 23(10), 5048 (1981)
29. X. L. Yuan, M. A. Xue, W. Chen, and T. Q. An, Concentration-dependent crystal structure, elastic constants

and electronic structure of Zr_xTi_{1-x} alloys under high pressure, *Front. Phys.* 9(2), 219 (2014)

30. Y. Y. Qi, Z. W. Niu, C. Cheng, and Y. Cheng, Structural and elastic properties of Ce_2O_3 under pressure from LDA+U method, *Front. Phys.* 8(4), 405 (2013)
31. B. G. Pfrommer, M. Cote, S. G. Louie, and M. L. Cohen, Relaxation of crystals with the quasi-Newton method, *J. Comput. Phys.* 131(1), 233 (1997)
32. B. B. Karki, G. J. Ackland, and J. Crain, Elastic instabilities in crystals from ab initio stress-strain relations, *J. Phys.: Condens. Matter* 9(41), 8579 (1997)
33. R. M. Wentzcovitch, N. L. Ross, and G. D. Price, Ab initio study of $MgSiO_3$and $CaSiO_3$ perovskites at lower-mantle pressures, *Phys. Earth Planet. Inter.* 90(1–2), 101 (1995)
34. Z. L. Lv, Y. Cheng, X. R. Chen, and G. F. Ji, Electronic, elastic and thermal properties of $SrCu_2As_2$ via first principles calculation, *J. Alloys Compd.* 570, 156 (2013)
35. R. Hill, The elastic behaviour of a crystalline aggregate, *Proc. Soc. London A* 65(5), 349 (1952)
36. M. A. Blanco, E. Francisco, and V. Luana, GIBBS: isothermal-isobaric thermodynamics of solids from energy curves using a quasi-harmonic Debye model, *Comput. Phys. Commun.* 158(1), 57 (2004)
37. M. Flórez, J. M. Recio, E. Francisco, M. A. Blanco, and A. M. Pendas, First-principles study of the rocksalt-cesium chloride relative phase stability in alkali halides, *Phys. Rev. B* 66(14), 144112 (2002)
38. E. Francisco, M. A. Blanco, and G. Sanjurjo, Atomistic simulation of SrF_2 polymorphs, *Phys. Rev. B* 63(9), 094107 (2001)
39. D. Vogel, P. Kruger, and J. Pollmann, Structural and electronic properties of group-III nitrides, *Phys. Rev. B* 55(19), 12836 (1997)
40. G. K. H. Madsen, Automated search for new thermoelectric materials: The case of LiZnSb, *J. Am. Chem. Soc.* 128(37), 12140 (2006)
41. F. D. Murnaghan, The compressibility of media under extreme pressures, *Proc. Natl. Acad. Sci. USA* 30(9), 244 (1944)
42. M. P. Ghimire, T. P. Sandeep, T. P. Sinha, and R. K. Thapa, First principles study of the electronic and magnetic properties of semi-Heusler alloys NiXSb (X = Ti, V, Cr and Mn), *J. Alloys Compd.* 509(41), 9742 (2011)
43. S. L. Shang, A. Saengdeejing, Z. G. Mei, D. E. Kim, H. Zhang, S. Ganeshan, Y. Wang, and Z. K. Liu, First-principles calculations of pure elements: Equations of state and elastic stiffness constants, *Comput. Mater. Sci.* 48(4), 813 (2010)
44. P. Wang, Y. Cheng, X. H. Zhu, X. R. Chen, and G. F. Ji, First principles investigations on elastic and electronic properties of $BaHfN_2$ under pressure, *J. Alloys Compd.* 526, 74 (2012)
45. Y. Fan, Y. N. Osetsky, S. Yip, and B. Yildiz, Onset mechanism of strain-rate-induced flow stress upturn, *Phys. Rev. Lett.* 109(13), 135503 (2012)
46. Y. Fan, Y. N. Osetskiy, S. Yip, and B. Yildiz, Mapping strain rate dependence of dislocation-defect interactions by atomistic simulations, *Proc. Natl. Acad. Sci. USA* 110(44), 17756 (2013)
47. P. Ravindran, L. Fast, P. A. Korzhavyi, B. Johansson, J. Wills, and O. Eriksson, Density functional theory for calculation of elastic properties of orthorhombic crystals: Application to $TiSi_2$, *J. Appl. Phys.* 84(9), 4891 (1998)
48. J. He, E. Wu, H. Wang, R. Liu, and Y. Tian, Ionicities of boron-boron bonds in B_{12} icosahedra, *Phys. Rev. Lett.* 94(1), 015504 (2005)
49. S. F. Pugh, Relations between the elastic moduli and the plastic properties of polycrystalline pure metals, *Philos. Mag.* 45(367), 823 (1954)
50. R. S. Mulliken, Electronic population analysis on LCAO–MO molecular wave functions, *J. Chem. Phys.* 23(10), 1833 (1955)
51. M. D. Segall, R. Shah, C. J. Pickard, and M. C. Payne, Population analysis of plane-wave electronic structure calculations of bulk materials, *Phys. Rev. B* 54(23), 16317 (1996)